ADVANCED FUNCTIONAL MATERIALS
www.afm-journal.de

Highly Efficient and Fully Solution-Processed White Electroluminescence Based on Fluorescent Small Molecules and a Polar Conjugated Polymer as the Electron-Injection Material

*Shanfeng Xue, Liang Yao, Fangzhong Shen, Cheng Gu, Hongbin Wu, and Yuguang Ma**

Highly efficient and fully solution-processed white organic light-emitting diodes (WOLEDs) based on fluorescent small molecules and a polar conjugated polymer as electron-injection material are reported. The emitting layer in the WOLEDs is a blend of new blue-, green-, and red-fluorescent small molecules, with a blending ratio of 100:0.4:0.8 (B/G/R) by weight, and a methanol/water soluble conjugated polymerpoly[(9,9-bis(30-(*N*,*N*-dimethylamino)propyl)-2,7-fluorene)-alt-2,7-(9,9-dioctylfluorene)] (PFN) acts as the electron-injection layer (EIL). All the organic layers are spin-coated from solution. The device exhibits pure white emission with a maximum luminous efficiency of 9.2 cd A^{-1} and Commission Internationale d'Eclairage Coordinates of (0.35, 0.36). PFN acting as the EIL material plays a key role in the improvement of the device performance when used in solution-processed small-molecule WOLEDs.

1. Introduction

White organic light-emitting diodes (WOLEDs) have attracted considerable attention due to their potential applications in backlight for liquid crystal display, and light sources for indoor lighting.[1–3] In order to generate the desired white-light emission, several methods and technologies have been developed.[4–13] For small molecule-based devices, the most ordinary fabrication method is the sequential deposition of multiple layers, such that layer emits a single-color of light, or to simultaneously deposit different-color materials in one layer.[14,15] Recently, WOLEDs fabricated from solution-processed small molecules, like polymer materials, have aroused great interest in the organic optoelectronic fields because of the low cost of solution-processing techniques, and the high performance arising from the well-defined and contrivable structures, and high purity of small molecules. Generally, small-molecular materials for solution-processed devices have requirements for some basic features, e.g., high solubility and glass state particularity for high quality films, and high photoluminescence (PL) quantum efficiency and carrier transporting ability for device operation. There have been case studies of high-performance spin-coated devices from small molecules and prototype display screens developed from ink-jet small molecules.[16,17] In principle, these solution-processed small-molecular materials should be suitable for fabricating WOLEDs through a blending of RGB emitters in one layer. Indeed, there have been some reports on solution-processed small-molecule WOLEDs.[18–20] Though a device with single-layer structure is encouraged because of its simplicity, it often shows low luminous efficiency due to inefficient/unbalanced carrier injection from electrodes into the emitting layer. The multilayer heterostructure has become a basic design feature to enhance the efficiency and stability of organic solid-state devices. For solution-processed small-molecular devices, multilayer structures are also needed to improve device performance. A vacuum-deposited 1,3,5-tris(1-phenyl-1H-benzo[d]imidazol-2-yl)benzene (TPBi) layer as hole-blocking/electron-transporting layer between the emitting layer and metal cathode is frequently used in solution-processed small-molecular devices, which leads to increased efficiency but at the expense of increased cost and complexity. The preparation of fully solution-processed multilayer structures is a challenge due to resolvation of subsequent layers. One approach to overcome this is to utilize materials with great differences of solubility in organic solvents versus methanol/water.

Recently, the use of a methanol/water-soluble conjugated polymer poly[(9,9-bis(30-(*N*,*N*-dimethylamino)propyl)-2,7-fluorene)-*alt*-2,7-(9,9-dioctylfluorene)] (PFN) as electron-injection layer (EIL) in polymer-based WOLEDs was developed by Cao and co-workers.[21,22] PFN is soluble in water and polar solvents and allow fabrication of multilayer device structures by solution-processing methods that do not perturb underlying layers. When a thin PFN layer is inserted between the emitting layer and cathode, efficient electron-injecting is possible from stable high-work-function metals.

Dr. S. F. Xue, Mr. L. Yao, Dr. F. Z. Shen, Dr. C. Gu, Prof. Y. G. Ma
State Key Lab of Supramolecular Structure and Materials
Jilin University
2699 Qianjin Avenue, Changchun, 130012, P. R. China
E-mail: ygma@jlu.edu.cn
Prof. H. B. Wu
Key Laboratory of Specially Functional Materials
South China University of Technology,
Guangzhou, 510640, P. R. China

DOI: 10.1002/adfm.201102338

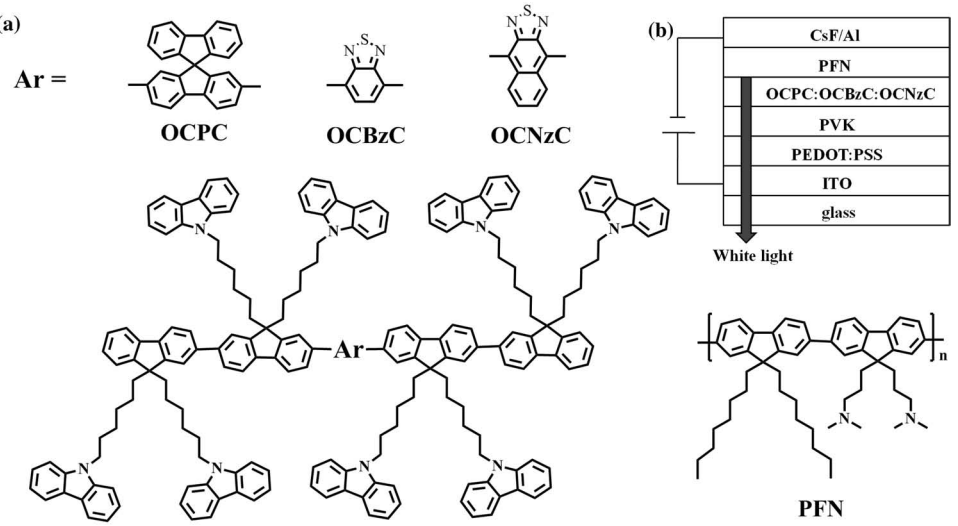

Scheme 1. a) The chemical structures of OCPC, OCBzC, and OCNzC. b) Schematic of the multilayer device structure.

In this work, we present the fabrication and characteristics of fully solution-processed small-molecule WOLEDs based on fluorescent small molecules (OCNzC (red), OCBzC (green), and OCPC (blue)) and a methanol/water soluble PFN as electron-injecting layer. To the best of our knowledge, the performance is the best ever reported for solution-processed fluorescent small-molecule WOLEDs via fully solution-processing techniques.

2. Results and Discussion

Recently, a series of solution-processed small-molecular materials named 4,9-bis(9,9,9′,9′-tetrakis(6-(9H-carbazol-9-yl)hexyl)-9H,9′H-[2,2′-bifluoren]-7-yl) naphtho[2,3-c][1,2,5] thiadiazole (OCNzC, red), 4,7-bis(9,9,9′,9′-tetrakis(6-(9H-carbazol-9-yl) hexyl)-9H,9′H-[2,2′-bifluoren]-7-yl) benzo[c][1,2,5] thiadiazole (OCBzC, green), and 2‴,7‴-bis(9,9,9′,9′-tetrakis(6-(9H-carbazol-9-yl)hexyl)-9H,9′H-[2,2′-bifluoren]-7-yl)-9,9‴-spirobi [fluorene] (OCPC, blue) have been synthesized by our group (details are given in the Supporting Information, see Scheme S1), the chemical structures of which are shown in **Scheme 1** a. The basic characteristics of this series of small-molecule materials are: i) high solubility, c.a., 30 mg mL^{-1} in *p*-xylene; ii) fully glass-like morphology in the solid, with a glass transition temperature (T_g) over 100 °C; iii) high photoluminescence (PL) quantum efficiency in solid state, e.g., 0.99 for OCPC. Thus, the materials meet the basic requirements for solution-processed fluorescent small-molecular OLEDs. Blends of OCPC, OCBzC, and OCNzC were used as the emission materials layer (EML) via solution-processing. As emission of individual colors (red (R), green (G), and blue (B)) is carefully controlled by an appropriate blending ratio, white-light emission can be obtained with a device structure of ITO/PEDOT:PSS (40 nm)/PVK (40 nm)/EML (≈50 nm)/CsF (1.5 nm)/Al (120 nm) (Device A). With a blend concentration of 100:0.4:0.8 (B/G/R) by weight, the white EL spectra show very balanced RGB distribution and full coverage of the whole visible range. Such a device exhibits a maximum luminance (*L*) of 5500 cd m^{-2} at 10.25 V, a maximum luminous efficiency (*LE*) of 4.4 cd A^{-1} and a maximum power efficiency (*PE*) of 2.6 lm W^{-1} at 2.31 mA cm^{-2}. Although this simple device showed quite good results, we believe that there is great potential to further improve device performance. Energy level analysis indicates that the highest occupied molecular orbital (HOMO) level of OCPC (–5.43 eV) is close to that of the anode (poly(3,4-ethylenedioxythiopene):poly(styrenesulfonate) (PEDOT:PSS)/indium tin oxide (ITO), –5.2 eV), while a higher barrier (2.01 eV) exists between OCPC and the cathode (CsF/Al) (see Figure S1 in the Supporting Information). This may induce holes to dominate in the emitting layer. In order to make the number of holes and electrons more balanced, a hole-blocking/electron-transporting layer between the emitting layer and metal cathode is needed in the device structure.

As the results above indicate, the choice of suitable electron-injection material and the building of complex films are important in such solution-processed devices. Next, methanol/water soluble conjugated polymer PFN as the EIL was studied. PFN is soluble in water and polar solvents and so allows fabrication of multilayer device structures by solution-processing methods that do not perturb underlying layers. In this approach, the preparation of the composite films is the critical problem. In order to prevent mixing between EML and the adjacent electron-injection layer (PFN), first of all, a thermal annealing treatment was used for EML at 70 °C for 20 min, making the EML film more solid and reduce corrosion of the film when the subsequent layer (PFN) was spin-coated. Next, the thin PFN film of 20 nm was deposited onto the EML by spin-coating from methanol solution. After that, thermal annealing at 80 °C for 10 min was applied. **Figure 1**a and b show atomic force microscopy (AFM) images of the EML atop ITO/PEDOT:PSS/poly(*N*-vinylcarbazole) (PVK) and the PFN layer atop ITO/PEDOT:PSS/PVK/EML. The results indicate that the PFN layer has no clear effects on the surface morphology. The EML film is pinhole-free and quite smooth with a surface roughness (root-mean-square) of approximately 0.41 nm. The surface roughness of the PFN layer decreases slightly to around 0.32 nm as compared to the

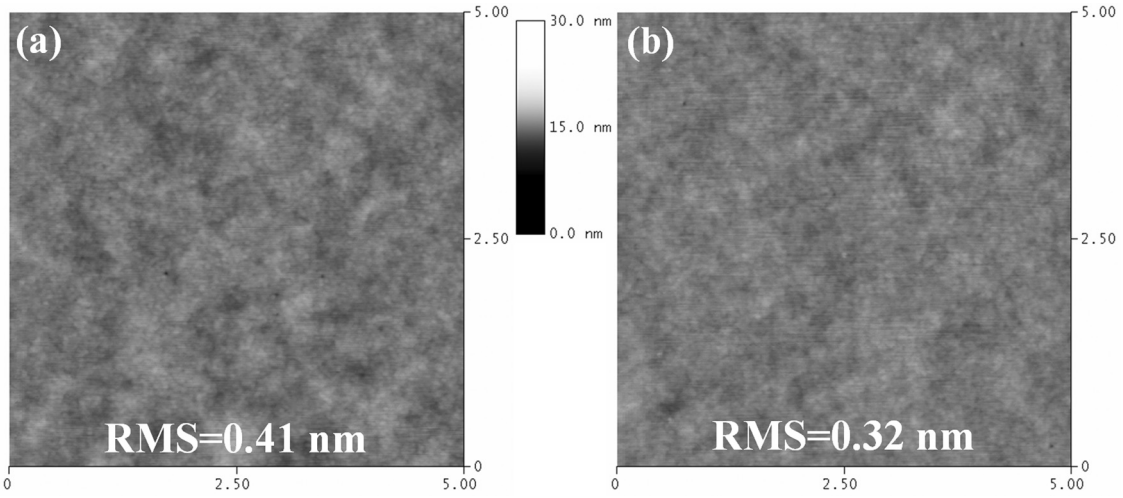

Figure 1. 5 μm × 5 μm AFM images of: a) the EML surface deposited atop ITO/PEDOT:PSS/PVK, and, b) the PFN surface deposited atop ITO/PEDOT:PSS/PVK/EML.

EML. Thus, such a process can provide good composite film without perturbing the underlying layers.

When the PFN was introduced to the device with structure ITO/PEDOT:PSS (40 nm)/PVK (40 nm)/EML (~50 nm)/PFN (20 nm)/CsF (1.5 nm)/Al (120 nm) (Device B) by solution-processing (a schematic of the multilayer device structure is shown in Scheme 1 b), it exhibited excellent performance. **Figure 2** shows: a) the current density–luminance–voltage (*J–L–V*), and, b) the luminous efficiency–power efficiency–current density (*LE–PE–J*) characteristics of devices A and B; detailed data are listed in **Table 1**. Device B shows a turn-on voltage of 3.75 V, lower than that of device A (4.25 V). The device has a maximum *L* of 16 000 cd m^{-2} at 9.75 V, a maximum LE of 9.2 cd A^{-1} and a maximum PE of 6.1 lm W^{-1} at a current density of 1.0 mA cm^{-2}. Note that the efficiency for device B at a luminance of 1000 cd m^{-2} is still high (6.6 cd A^{-1}). This performance is among the best ever reported for solution-processed fluorescent small-molecule WOLEDs fabricated via fully solution-processed techniques. The device efficiency was doubled when PFN was introduced, demonstrating that PFN works efficiently as an EIL for small molecule-based WOLEDs. Thus, more balanced hole and electron injection is expected to be responsible for the improved device performance.

In order to understand the enhanced electron injection at PFN/CsF/Al interfaces, photovoltaic measurements were performed to determine the built-in potentials (V_{bi}) across each device, which directly reflect the shift of the effective work function of the cathodes; thus, the contact barrier can be evaluated.[23] The built-in potentials can be estimated from the open-circuit voltage (V_{oc}) of devices, obtained from the *I–V* curves under illumination. Based on the electrochemical measurements of organic emitting material (OCPC) (see Figure S2 in the Supporting Information), and built-in potentials (V_{bi}) estimated from photovoltaic measurements, the energy levels of incorporated PFN layer device are shown in **Figure 3**b. As shown in Figure 3a and b, the obtained V_{oc} of these devices are 1.4 V (Device A) and 2.25 V (Device B), indicating that the PFN/CsF/Al structure indeed reduces the electron injection

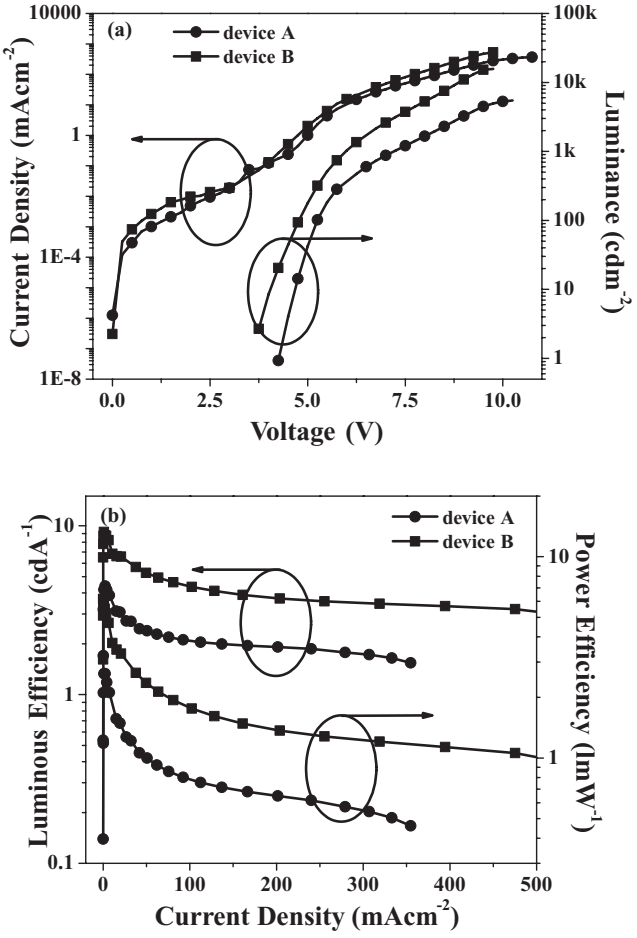

Figure 2. a) The current density–luminance–voltage (*J–L–V*), and, b) the luminous efficiency–power efficiency–current density (*LE–PE–J*) characteristics of devices with the structures ITO/PEDOT:PSS(40 nm)/PVK(40 nm)/EML(≈50 nm)/CsF(1.5 nm)/Al(120 nm) (device A), and the ITO/PEDOT:PSS(40 nm)/PVK(40 nm)/EML(≈50 nm)/PFN(20 nm)/CsF(1.5 nm)/Al(120 nm) (device B).

Table 1. Devices performance for WOLEDs at the same doping ratio and different device structures. Device structure of A: ITO/PEDOT:PSS/PVK/EML/CsF/Al. Device structure of B: ITO/PEDOT:PSS/PVK/EML/PFN/CsF/Al.

Device	LE_{Max} [a]	PE_{Max} [b]	L_{Max} [c]	Device performance at 1000 cd m^{-2}		CIE [d]		CCT	CRI [d]
	[cd A^{-1}]	[lm W^{-1}]	[cd m^{-2}]	*LE* [cd A^{-1}]	*PE* [lm W^{-1}]	*x*	*y*	*K*	
A	4.4	2.6	5500	2.5	1.1	0.35	0.37	4979	80
B	9.2	6.1	16 000	6.6	3.5	0.35	0.36	4694	83

[a]Maximal front viewing luminous efficiency in cd A^{-1}; [b]Maximum power efficiency; [c]Maximum luminance; [d]Observer: 2°; obtained at 11 mA cm^{-2}.

barrier and realizes more efficient electron injection than CsF/Al in solution-processed small-molecule WOLEDs. At present, the origin of the PFN interfacial layer for lowing the electron injection barrier is not very clear. We suspect the formation of interfacial dipole on the PFN/cathode interface may lead to enhanced V_{bi} and a lower electron injection barrier. We have made the small angle X-ray diffraction and electro-absorption measurements for PFN/cathode interface,[21,24,25] which provide the evidences for the alignment of PFN chain and the formation of interfacial electrical dipole.

The EL spectra of device B recorded between current densities of 21 to 105 mA cm^{-2} are shown in **Figure 4**a. Three intense

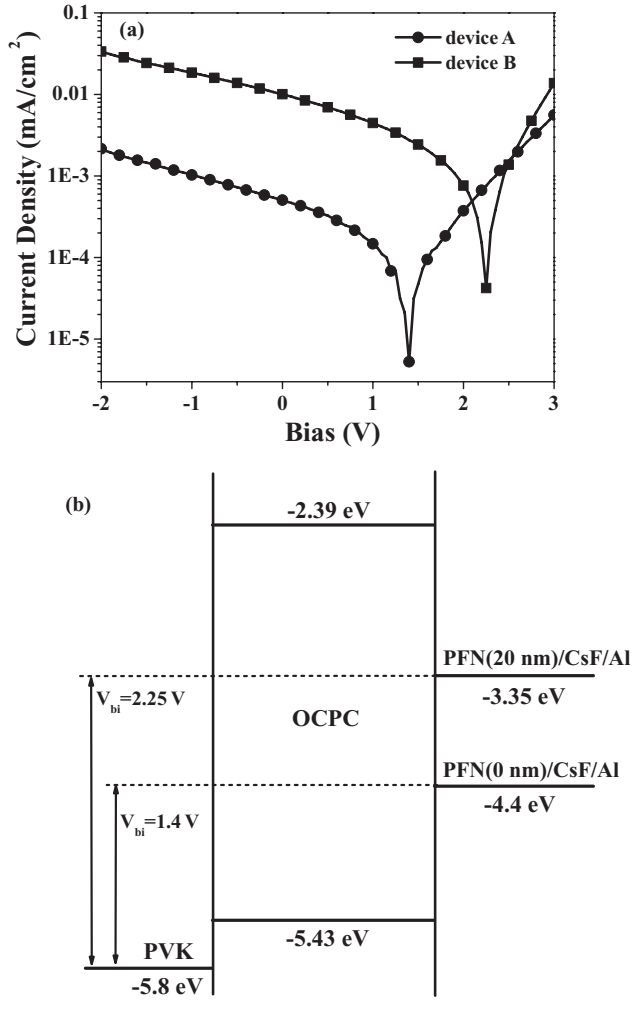

Figure 3. a) Photovoltaic characteristics of device A (ITO/PEDOT:PSS(40 nm)/PVK(40 nm)/EML(≈50 nm)/CsF(1.5 nm)/Al(120 nm)) and device B (ITO/PEDOT:PSS(40 nm)/PVK(40 nm)/EML(≈50 nm)/PFN(20 nm)/CsF(1.5 nm)/Al(120 nm)). b) Schematic diagram of the relative energy levels at flat band condition for devices.

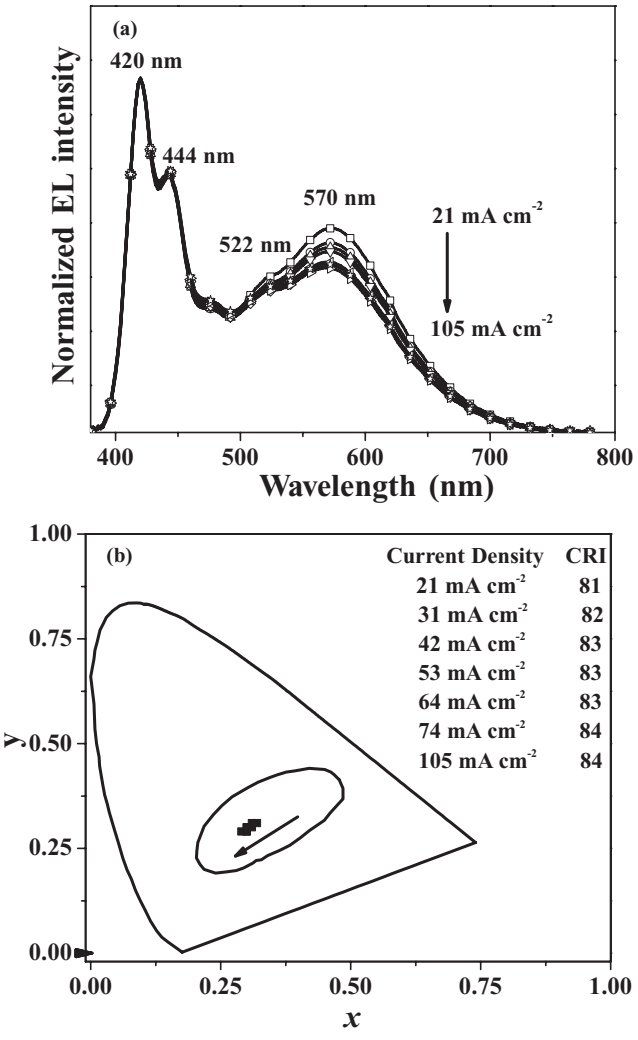

Figure 4. a) EL spectra and b) color rendering index (CRI) of device B (ITO/PEDOT:PSS(40 nm)/PVK(40 nm)/EML(≈50 nm)/PFN(20 nm)/CsF(1.5 nm)/Al(120 nm)) under different current densities (21 to 105 mA cm^{-2}).

peaks around 420, 522, and 570 nm were clearly observed, which can be attributed to the emission from the emitting core of OCPC, OCBzC, and OCNzC, respectively. Device B showed excellent spectral stability, and the EL spectral shape did not change much with increasing current density. The Commission Internationale de'Eclairage (CIE) coordinates, the color correlated temperature (CCT), and the color rendering index (CRI) are the three critical parameters characterizing the color quality of white lighting sources. These parameters are summarized in Table 1. As shown in Table 1, the white EL spectra show CIE coordinates of (0.35, 0.36), which is quite close to the standard white light point of (0.33, 0.33). Our device exhibits the CRI of 83, which can be employed for indoor-lighting applications (CRI ≥ 80).[26] More details of the CIE coordinates and CRI at varied driving current density are included in Figure 4b.

3. Conclusions

In summary, combining the solution processing capability of PFN with the common features of small molecules, WOLEDs were fabricated having all layers prepared by solution-processing techniques. The devices showed efficient white light emission from the blending of fluorescent small-molecule light-emitting layers. The introduction of PFN as EIL improves the device performance with higher luminous efficiency (9.2 cd A^{-1}), power efficiency (6.1 lm W^{-1}), and luminance (16 000 cd m^{-2}) compared to the previous reports. Our investigation demonstrates that it is achievable to fabricate efficient small-molecule WOLEDs via fully solution-processing techniques, and the WOLEDs exhibit a huge potential for low-cost large-area manufacturing.

4. Experimental Section

Materials: The small-molecules OCPC, OCBzC, and OCNzC used as emisive materials were synthesized in our laboratory. PFN[22] was used as electron-injecting material in WOLEDs. The chemical structures of these materials are shown in Scheme 1. PVK and cesium fluoride (CsF) were purchased from Aldrich. PEDOT:PSS (Baytron P 4083, Bayer AG) was purchased from H. C. Starck. Inc. These materials were used as received.

Instrumentation and Device Fabrication: ITO-coated glass with a sheet resistance of 15–20 Ω per square was used as the substrate. The substrate was prepatterned by photolithography to give an effective device size of 19 mm^2, then cleaned in an ultrasonic bath with acetone, detergent, deionized water, and isopropanol in sequence, and finally dried in an oven. After oxygen plasma cleaning for 4 min, a 40 nm-thick PEDOT:PSS layer was first spin-coated on the ITO substrate from water solution and then dried by baking in a vacuum oven at 80 °C overnight. A 40 nm thick layer of PVK was subsequently spin-coated onto the top of the PEDOT:PSS layer from chlorobenzene solution, followed by thermal annealing at 120 °C for 10 min. On the top of that, the small-molecule emitting layer (EML) was spin-coated from OCPC:OCBzC:OCNzC (blending ratio 100:0.4:0.8 by weight) *p*-xylene solution form an approximately 50 nm thick film. Next, a thin PFN film of 20 nm was deposited onto the EML by spin-coating from methanol solution with a few drops of acetic acid. The thicknesses of these organic films were determined using a surface profiler (Tencor Alfa-Step 500). Finally a 1.5 nm thick CsF film and a 120 nm thick Al film were evaporated with a shadow mask to form the top electrode, at a base pressure of 3×10^{-4} Pa. The thickness of the evaporated cathodes was monitored by a quartz crystal thickness/ratio monitor (Model: STM-100/MF, Sycon). The device fabrication, except PEDOT:PSS coating, was carried out in a nitrogen atmosphere glove-box (Vacuum Atmosphere Co.) containing less than 10 ppm oxygen and moisture.

The current density–luminance–voltage (*J–L–V*) characteristics were measured by a Keithley 236 source measurement unit. The EL spectra and CIE coordination characteristics of WOLEDs were measured by using a PR-705 Spectroscan spectrometer. For photovoltaic measurement, the photocurrent–voltage characteristics were recorded with a Keithley 2410 source unit under the white-light illumination of a xenon lamp (Thermo Oriel 150 W). Open-circuit voltage (V_{OC}) of devices was defined as the voltage at which the corresponding photocurrent is equal to zero. The atomic force microscopy (AFM) image was recorded on a Seiko SPA 400 with an SPI 3800 probe station in tapping mode (dynamic force mode). Electrochemical measurements were performed with a BAS 100W Bioanalytical System, a glass-carbon disk electrode was used as the working electrode, a Pt wire as the counter electrode, Ag/AgCl as the reference electrode and Bu_4NClO_4 (0.1 M) in acetonitrile as electrolyte.

Supporting Information

Supporting Information is available from the Wiley Online Library or from the author.

Acknowledgements

This work was supported by grants from the Natural Science Foundation of China (20834006) and the Ministry of Science and Technology of China (2009CB623605).

Received: September 30, 2011
Revised: November 21, 2011
Published online: January 18, 2012

[1] H. B. Wu, L. Ying, W. Yang, Y. Cao, *Chem. Soc. Rev.* **2009**, *38*, 3391.
[2] B. W. D'Andrade, S. R. Forrest, *Adv. Mater.* **2004**, *16*, 1585.
[3] S. Kim, J. Seo, H. K. Jung, J. J. Kim, S. Y. Park, *Adv. Mater.* **2005**, *17*, 2077.
[4] M. Berggren, O. Inganäs, G. Gustafsson, J. Rasmusson, M. R. Andersson, T. Hjertberg, O. Wennerström, *Nature* **1994**, *372*, 444.
[5] X. Gong, W. L. Ma, J. C. Ostrowski, G. C. Bazan, D. Moses, A. J. Heeger, *Adv. Mater.* **2004**, *16*, 615.
[6] J. S. Huang, G. Li, E. Wu, Q. F. Xu, Y. Yang, *Adv. Mater.* **2006**, *18*, 114.
[7] Y. S. Park, J. W. Kang, D. M. Kang, J. W. Park, Y. H. Kim, S. K. Kwon, J. J. Kim, *Adv. Mater.* **2008**, *20*, 1957.
[8] C. Gu, T. Fei, L. Yao, Y. Lv, D. Lu, Y. G. Ma, *Adv. Mater.* **2011**, *23*, 527.
[9] Y. H. Xu, J. B. Peng, J. X. Jiang, W. Xu, W. Yang, Y. Cao, *Appl. Phys. Lett.* **2005**, *87*, 193502.
[10] H. B. Wu, J. H. Zou, F. Liu, L. Wang, A. Mikhailovsky, G. C. Bazan, W. Yang, Y. Cao, *Adv. Mater.* **2008**, *20*, 696.
[11] X. Gong, S. Wang, D. Moses, G. C. Bazan, A. J. Heeger, *Adv. Mater.* **2005**, *17*, 2053.
[12] Q. Wang, J. Q. Ding, D. G. Ma, Y. X. Cheng, L. X. Wang, F. S. Wang, *Adv. Mater.* **2009**, *21*, 2397.
[13] J. Liu, Q. G. Zhou, Y. X. Cheng, Y. H. Geng, L. X. Wang, D. G. Ma, X. B. Jing, F. S. Wang, *Adv. Mater.* **2005**, *17*, 2974.
[14] Y. Sun, N. C. Giebink, H. Kanno, B. Ma, M. E. Thompson, S. R. Forrest, *Nature* **2006**, *440*, 908.
[15] J. Kido, M. Kimura, K. Nagai, *Science* **1995**, *267*, 1332.
[16] B. J. Gans, P. C. Duineveld, U. S. Schubert, *Adv. Mater.* **2004**, *16*, 203.

[17] C. R. McNeill, N. C. Greenham, *Adv. Mater.* **2009**, *21*, 3840.
[18] L. D. Hou, L. Duan, J. Qiao, D. Q. Zhang, G. F. Dong, L. D. Wang, Y. Qiu, *Org. Electron.* **2010**, *11*, 1344.
[19] J. H. Jou, M. C. Sun, H. H. Chou, C. H. Li, *Appl. Phys. Lett.* **2005**, *87*, 043508.
[20] D. D. Wang, Z. X. Wu, X. W. Zhang, B. Jiao, S. X. Liang, D. W. Wang, R. L. He, X. Hou, *Org. Electron.* **2010**, *11*, 641.
[21] H. B Wu, F. Huang, Y. Q. Mo, W. Yang, D. L. Wang, J. B. Peng, Y. Cao, *Adv. Mater.* **2004**, *16*, 1826.
[22] F. Huang, H. B. Wu, D. L. Wang, W. Yang, Y. Cao, *Chem. Mater.* **2004**, *16*, 708.
[23] F. Huang, P. I. Shih, C. F. Shu, Y. Chi, A. K. Y. Jen, *Adv. Mater.* **2009**, *21*, 361.
[24] H. B Wu, F. Huang, J. B. Peng, Y. Cao, *Org. Electron.* **2005**, *6*, 118.
[25] Z. C. He, C. M. Zhong, X. Huang, W. Y. Wong, H. B. Wu, Li. W. Chen, S. J. Su, Y. Cao, *Adv. Mater.* **2011**, *23*, 4636.
[26] M. C. Gather, A. Köhnen, K. Meerholz, *Adv. Mater.* **2011**, *23*, 233.